A methodology to assess crack-sealing effectiveness of crystalline admixtures under repeated cracking-healing cycles

Estefanía Cuenca *, Antonio Tejedor, Liberato Ferrara

Department of Civil and Environmental Engineering, Politecnico di Milano, Piazza Leonardo da Vinci, 32, 20133 Milan, Italy

This paper analyzes the autogenous and stimulated self-sealing capacity of steel fiber reinforced con-cretes, with and without crystalline admixtures, under repeated cracking and healing cycles. To this pur-pose, the performance under cracking and healing cycles was investigated on 150 × 150 × 50 mm^3 specimens, cracked by means of an indirect tensile test called Double Edge Wedge Splitting (DEWS) test. Two concrete mixes (with and without crystalline admixtures) and three healing exposure conditions were investigated: water immersion, open-air exposure and wet/dry cycles. Initially, the specimens were cracked up to a crack opening of 0.25 mm and were then subjected to the different aforementioned expo-sure conditions for 1, 3 and 6 months. At the end of each period, the specimens were cracked again and were subjected to the different exposure conditions for an additional 1 or 2 months, repeating the crack-ing and healing procedure up until a total duration of one year. The crack closure was analyzed using image processing methods. The results show that, for the same healing period, the specimens immersed in water reached the largest crack closures. In addition, it was observed that the crystalline admixture may favor long-term self-sealing capacity under repeated cracking and healing events.

Keywords:
Self-sealing
Crystalline admixtures
Repeatability Durability
Fiber reinforced concrete
Cracking-healing cycles

1. Introduction

The increasing concern about a responsible use of raw materials and the need to guarantee a higher and tailored level of material and structural performance in engineering applications for longer times has promoted a huge amount of research on the challenging topic of self-healing (cement-based) construction materials. RILEM TC 221 [1] defines self-healing as "any process by the material itself involving the recovery and hence improvement of a perfor-mance, after an earlier action had reduced the performance of the material".

It is well known that, by itself, concrete has some moderate self-healing capabilities (autogenous healing). This is closely related to the fact that, in most concretes, approximately 20–30% of the cement particles remain anhydrous. When a crack appears, such anhydrous particles come into contact with water or moisture and react with it creating hydration products that contribute to the closure of the crack [2–5]. Moreover, $Ca(OH)_2$ particles pro-duced by cement hydration may release calcium ions which, react-ing with carbonate ions in water or carbon dioxide in air, form calcium carbonate precipitates, also contributing to close the cracks. This type of self-healing is known as "autogenous healing", which occurs when cracks are healed by usual constituents of the cementitious matrix and, therefore, materials that are not specifically added to the same matrix for self-healing purposes (this is, own generic materials) [1,6–9]. On the other hand, the healing process is called "engineered healing" when specific engineered additions designed to promote it are purposely added to the concrete mix-design [10–16]. Tailored additions such as silica fume [17],

* Corresponding author.
E-mail address: estefania.cuenca@polimi.it (E. Cuenca).

Published Journal Article available at: https://doi.org/10.1016/j.conbuildmat.2018.05.261

crystalline admixtures [11,12,18–21] and superabsorbent polymers [8,22–24] have been used to stimulate the autogenous self-healing capability of concrete mixtures.

In turn, the synergy between fiber reinforced cementitious composites (FRCCs) and self-healing techniques is giving rise to solutions with great potential [10] since fibers can improve the self-sealing process because of their ability to control the width and propagation of the cracks [4,6,7,12,18,25,9,14,26]. In fact, FRCCs are characterized by enhanced toughness due to the crack-bridging effects provided by fibers [27–37]. The test results indi-cate that the use of fibers reduce the maximum and average crack width, as well as the crack spacing [29,30].

It has been shown that cracks smaller than 30 μm (and in some cases even 50 μm) can be healed completely [5,24,38]. Subsequently, the next step would be to analyze if the sealing mechanism is maintained over time after several cracking-healing cycles (self-healing repeatability). Compared to the large number of investigations on self-healing [6,7,10,11,18,19,20,9] among others, studies on the persistence of the healing capacity under repeated cracking and healing events of self-healing FRCC are less numerous [22,39–42] which has motivated this research. Among the cited studies on the persistence of the healing capacity under repeated cracking events, it is worth recalling the works by Snoeck et al. [22] and Sahmaran et al. [39]. Snoeck et al. [22] studied the ability of repeatable promoted autogenous healing in fiber-reinforced materials with and without superabsorbent polymers (SAPs). To this purpose, the mechanical properties of the speci-mens were compared after two cycles of loading under a four-point-bending test. Results showed that the healed specimens regained up to 75% of their mechanical properties and, a partial additional regain in mechanical properties up to 66% was observed even second reloading of healed specimens. On the other hand, Sahmaran et al. [39] studied the self-healing ability of engineered cementitious composites (ECCs). To generate microcracks on spec-imens, a repeatedly preloading up to 70% of their deformation capacities was applied by means of dynamic modulus tests based on ASTM C215, after the mechanical tests specimens were sub-jected to a cyclic wet/dry conditioning period. The extend and rate of self-healing under repetitive preloading conditions was deter-mined by resonant frequency (RF) and rapid chloride permeability tests (RCPT). Results showed that ECC specimens can recover up to 85% of their initial RF values, even after six repeated cracking/heal-ing cycles. In addition, the maximum crack width observed was 190 μm, even after nine cracking/healing cycles.

As a matter of fact, in the analysis of the crack sealing capacity of any material, the main issue remains the observation and measurement of the crack width and of its evolution in the investigated scenario. In the last decade, with the improvement of the photogrammetric and image processing methods, several crack-detection and characterization algorithms have been developed [43]. These procedures can yield high precision results especially on surfaces with homogeneous texture and illumination [44]. The detection algorithm starts with the application of filters that smooth the error and enhance the edges [45]. Subsequently, the procedure that allows the identification of the crack is applied. The most prominent methods today are the so-called binarization algorithms [46]. These methods perform a classification of each pixel into two categories; white or black (crack or non-crack), based on the definition of a radiometric threshold [47]. The result of this process is called "segmented image". Finally, additional filtering allows the elimination of outliers. Several authors, such as [48–55] have made use of these digital image processing methods for the detection and quantification of cracks in concrete. The procedure must be adapted according to the characteristics to be obtained: width, length, depth or area of the crack, the latter being the most frequently chosen for the study of the time evolution of cracking. The accuracy in detecting such crack parameters (i.e. estimated crack parameter versus measured crack parameter) using image analysis techniques varies from 75% to 95% compared to manual visual perception measurements [43].

The main objective of this work is to analyze the repeatability of the self-sealing of fiber-reinforced concrete and how it is influenced by the addition of crystalline admixtures. Crack width was measured by means of image processing methods. The crack sealing capacity was quantified through the definition of suitable indices under each of the analyzed conditions and along the investigated cracking-healing cycles.

2. Experimental program

2.1. Mix design, materials characterization and test set-up

A conventional fiber reinforced concrete (FRC) mix was used in this research, with the composition shown in Table 1. Besides a reference mix, another mix (denoted as C.A. concrete) containing 0.8% by cement weight of a crystalline admixture (Penetron Admix ®) used as healing promoter was also produced, leaving the mix proportions substantially unaltered. The objective of this research was to analyze a typical fiber reinforced concrete used for structural applications, containing a typical quantity of steel macrofibers. Both mixes contained 40 kg/m^3 hooked-end steel fibers 60 mm long and 0.9 mm in diameter (fiber aspect ratio equal to 65).

The employed crystalline admixture (Penetron Admix ®), consists of a blend of cement, sand and microsilica. It reacts with the moisture in fresh concrete and with the products of cement hydration producing a non-soluble crystalline formation which promotes crack sealing. This product was analyzed by means of SEM and EDS analysis (Section 3.2). A detailed description of its morphology and composition can be found in [19].

The mechanical properties of the investigated FRC were measured at 3, 7, 28 and 56 days by means of compressive strength test

Table 1
Concrete mix design.

Constituent [kg/m^3]	Reference Concrete (Without crystalline admixtures)	C.A. Concrete (With crystalline admixtures)
Cement type II 42.5	360	
Water	180	
Superplasticizer	3.5	
Coarse aggregate 4–16 mm	1077	
Steel fibers, Dramix 5D 65/60BG	40	
Fine aggregate 0–4 mm	814	811
Crystalline admixture (Penetron Admix ®)	0	2.9

Table 2
Concrete mechanical properties. Average values in MPa.

Concrete	Age (days)	f_c (MPa)	f_{R1} (MPa)	f_{R2} (MPa)	f_{R3} (MPa)	f_{R4} (MPa)
Reference Concrete Without crystalline admixtures	**3**	–	6.05 ± 0.29	8.08 ± 0.12	7.79 ± 0.91	8.03 ± 0.21
	7	40.9 (3.70)	6.20 ± 0.45	8.03 ± 0.88	7.92 ± 0.01	6.62 ± 0.19
	28	46.6 (3.84)	7.60 (0.03)	8.38 (0.52)	8.46 (0.06)	8.14 (0.03)
	56	47.0 (3.83)	8.27 ± 0.26	10.45 ± 0.51	10.62 ± 0.87	9.00 ± 0.41
C.A. Concrete With crystalline admixtures	**3**	–	4.67 ± 0.13	6.80 ± 0.63	6.09 ± 0.15	5.72 ± 0.13
	7	34.6 (3.47)	6.38 ± 0.42	8.07 ± 0.82	7.86 ± 1.45	6.15 ± 0.61
	28	41.2 (3.62)	6.08 (0.80)	9.29 (0.75)	9.08 (0.32)	7.78 (0.94)
	56	41.0 (4.04)	5.44 ± 0.21	7.64 ± 0.50	8.29 ± 0.79	8.23 ± 0.93

(f_c) on 150 mm side cubes and flexural tests (EN 14651) on 150 × 150 × 600 mm^3 prism specimens. The specimens were cured in a moist room with a relative humidity of 95% and a temperature of 20 °C until the day of testing. From the flexural tests, the residual flexural tensile strength ($f_{R,j}$) at crack mouth opening displacements (CMOD) equal to 0.5, 1.5, 2.5 and 3.5 mm (j = 1, 2, 3, 4 respectively) were obtained. Table 2 shows the mechanical properties of both concrete mixes at different ages. The compressive strength values are the average of three nominally identical specimens (standard deviation in brackets), while for the residual flexural tensile strength 9 prismatic specimens were tested for each matrix (for a total of 18 specimens): 2 prismatic specimens were tested at 3 days, 7 days and 56 days, whereas the remaining 3 prismatic specimens were tested at 28 days. For the residual post-cracking strengths (Table 2), standard deviation (in brackets) is given when at least three specimens were tested, while in the other case, when only two specimens were tested, the result scatter in MPa is reported.

Once the beam specimens were tested, they were cut into slices according to two main directions to consider the effect of the fiber orientation as shown in Fig. 1. Because of the high flowability of the employed concretes, the casting of prismatic specimens was accomplished through a free flow parallel to the longer side of the formworks (Fig. 1b). This eased a preferential orientation of the fibers along the same direction. Due to the suitably conceived notched specimen geometry (Fig. 1c)

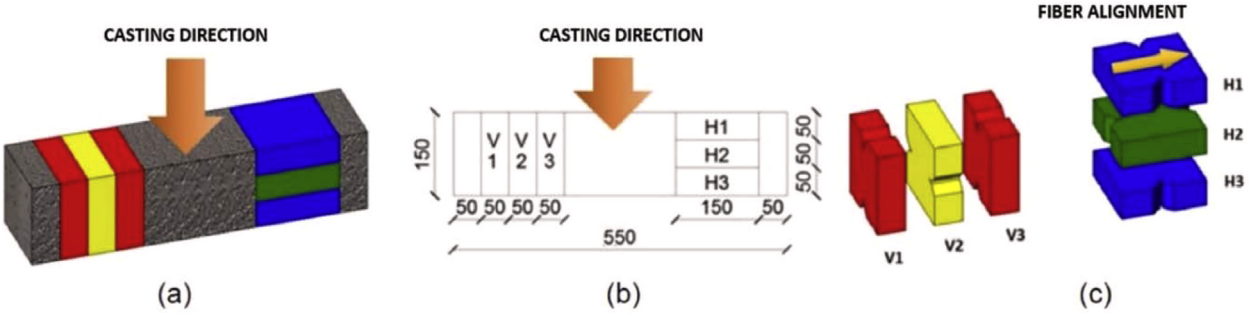

Fig. 1. Cutting scheme to obtain specimens for DEWS tests. Dimensions in mm.

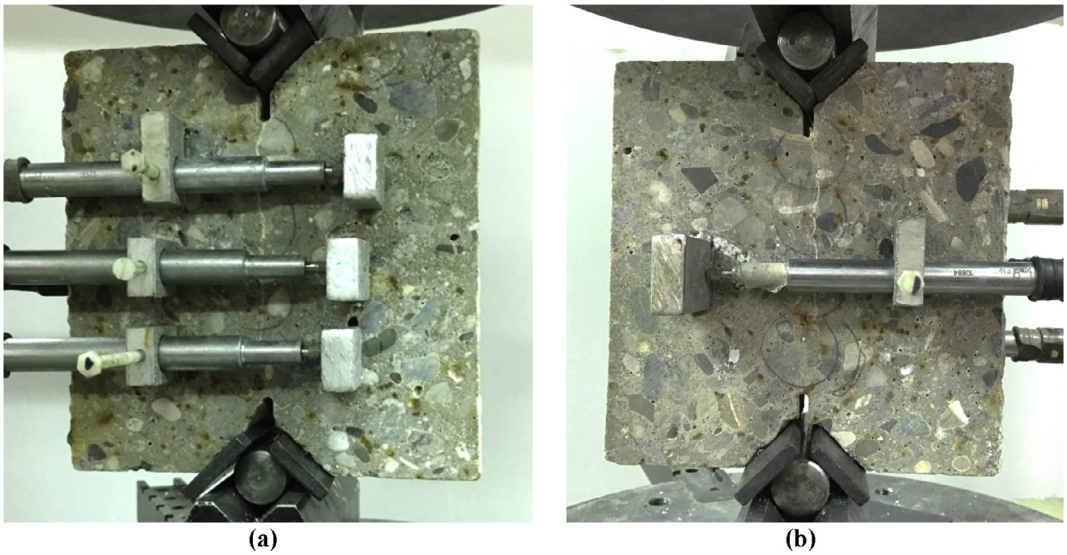

Fig. 2. Test set-up of Double edge wedge splitting (DEWS) tests: front (a) and rear face (b).

[56], it was possible to predetermine the fracture plane (critical section), in such a way that it resulted parallel or orthogonal to the flow direction and hence to the obtained preferential align-ment of the fibers. In this way, for specimens H1 and H3 the preferential alignment of fibers was orthogonal to the fracture plane; on the contrary, in specimens H2, V1, V2 and V3 the fibers did not cross the fracture plane orthogonally. To quantify the influence of the fiber orientation, some of the specimens were monotonically tested up to failure employing the Double Edge Wedge Splitting Test methodology [56]. The tests were carried out by controlling and measuring the residual tensile stress at different crack opening displacements (COD = 0.25, 0.5, 1.25 and 1.5 mm) along the ligament on both the front and rear face of the DEWS specimens, as shown in Fig. 2. The fibers which crossed the fracture plane were counted and, the fiber density per unit area of fracture surface was calculated. The relationship between the residual tensile stress and the fiber density is shown in Fig. 3. In all cases, a very good fitting was obtained, with moderate differences between the residual stresses at progressively increasing crack opening, as expectable because of the fiber pull-out nature of such stresses.

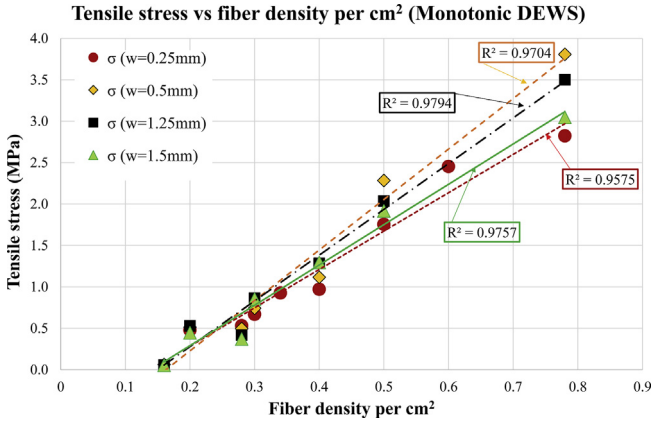

Fig. 3. Residual tensile stresses at different crack openings versus fiber density-monotonic tests.

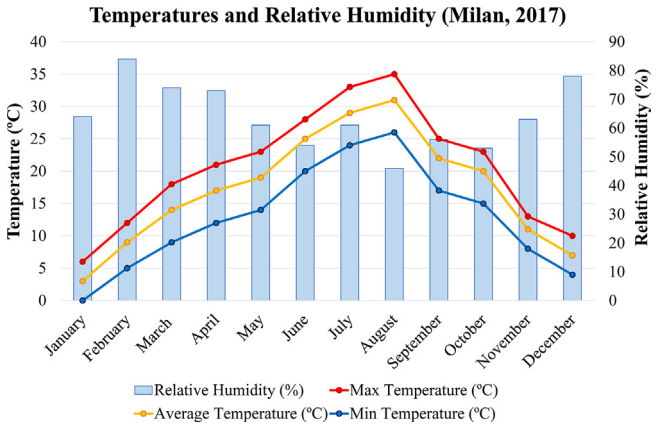

Fig. 4. Temperature and Relative Humidity variations throughout the year 2017 in Milan (Italy).

The remaining specimens were cured at 20 °C and 95% relative humidity up to an age of 4 months after casting, after which they were pre-cracked according to the same DEWS (Double Edge Wedge Splitting test) methodology [56].

Precrack tests were performed up to a crack opening displacement (COD) of 0.25 mm. This reference COD value was measured as the average between the 3 LVDTs on the front face of the specimen and the one on the rear face (Fig. 2). After the complete unloading (residual crack opening was in range of 0.20–0.30 μm for all the specimens), the cracks were photographed and the specimens were exposed to one of the following conditions: water immersion, open-air exposure, wet/dry cycles (4 days immersed in water and 3 days exposed to the open-air). As for the open-air exposure, the climate characteristics in Milan (Italy) during the one year long period of investigation, featured temperatures ranging between 3 and 31 °C and relative humidity between 46 and 84% (Fig. 4).

The scheme of the cracking-healing cycles is shown in Fig. 5. Three different experimental itineraries were clearly distinguished being the main difference the duration of the first healing treatment: FT-1 were those specimens whose initial treatment lasted 1 month, FT-3 were those in which it was 3 months and FT-6 were those in which it was 6 months. For example, the 23 DEWS specimens belonging to the FT-6 group were subjected to the following sequence: self-healing for 6 months in each of the 3 exposure environments + 0.25 mm cracking + self-healing for 1 month + 0.25 mm cracking + self-healing for 2 months + cracking of 0.25 mm + self-healing for 1 month + 0.25 mm cracking + self-healing for 2 months + cracking 0.25 mm, as indicated in Fig. 5.

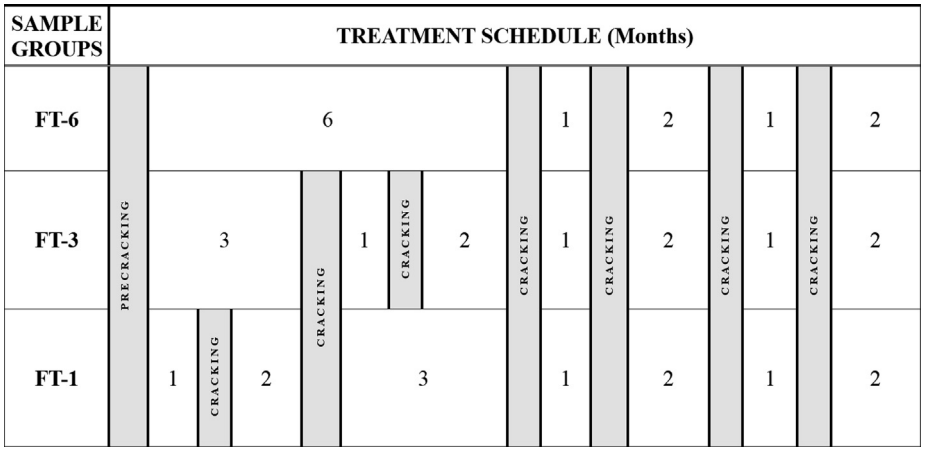

Fig. 5. Scheme of the testing-treatment campaign. Except for the first one, the rest of the healing treatments follow a regular scheme of 1 and 2 months.

After the first healing treatment the cracks of each sample group (FT-1, FT-3 and FT-6) were photographed once again. The cracking-healing cycle then started, consisting in further opening of the crack of additional 0.25 mm, followed by the healing period under the prescribed exposure conditions for, alternatively, 1 or 2 months, up to a total duration of one year after the pre-cracking (Fig. 5). A total number of 65 specimens was tested (Table 3). The final results were also supported by SEM observations and EDS analyses (Section 3.2).

Table 3
Number of samples for the different variables.

First healing treatment duration	# SAMPLES
1 month	22
3 months	20
6 months	23
Environmental exposure	**# SAMPLES**
Water	22
Open-air exposure	22
Wet/dry Cycles	21
Mix design	**# SAMPLES**
Reference Concrete (without crystalline admixtures)	33
C.A. Concrete (with crystalline admixtures)	32
Fiber Orientation	**# SAMPLES**
V (parallel)	23
H1,H3 (perpendicular)	26
H2 (parallel)	16
TOTAL	65

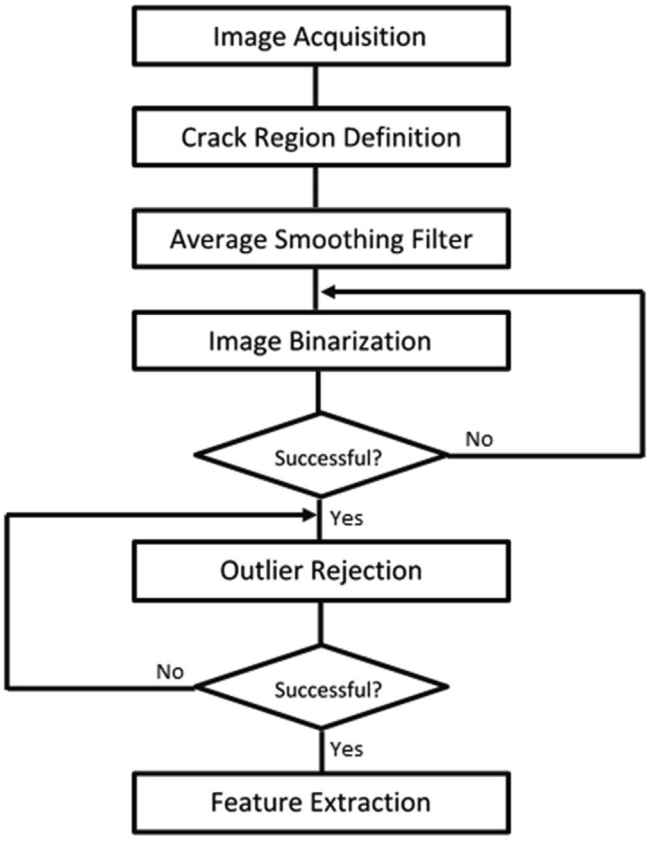

Fig. 7. Image analysis flowchart for the proposed crack detection method.

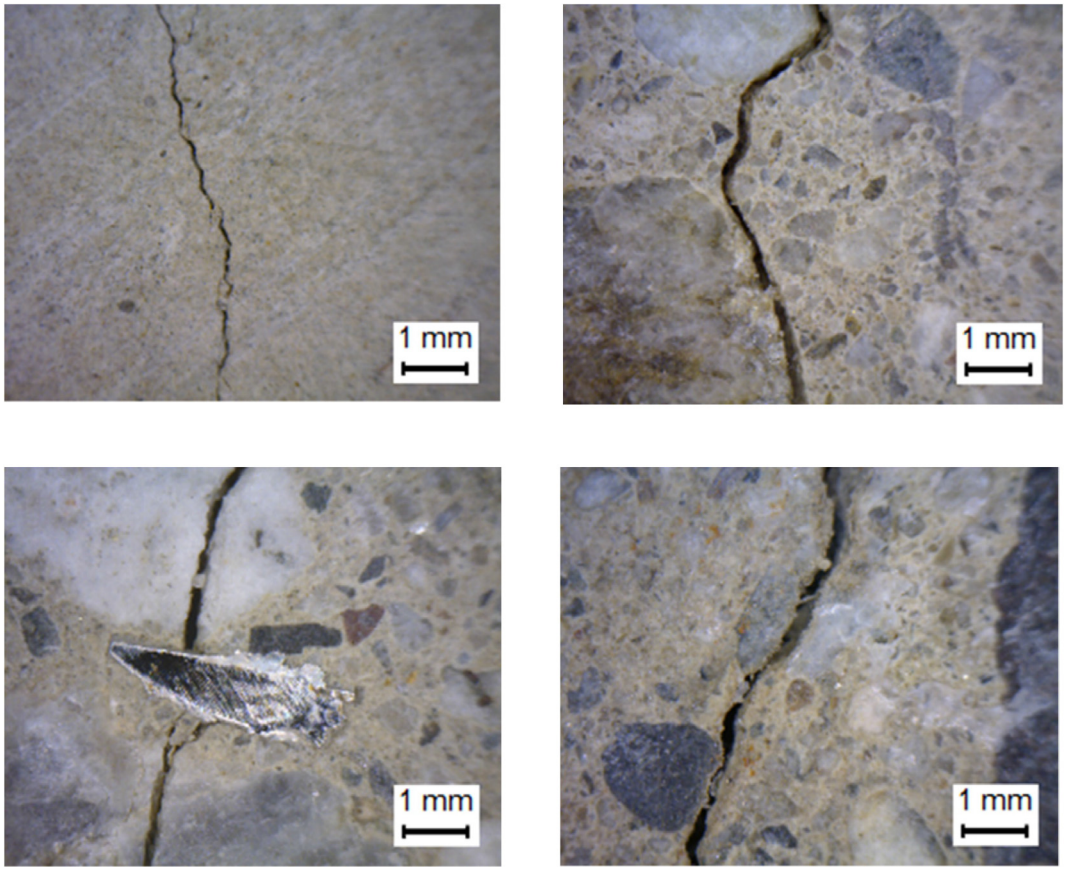

Fig. 6. Sample images at 56X magnification showing the variety of surface textures.

2.2. Image analysis methodology

The evaluation of the self-sealing efficiency has to start from the crack closure quantification, comparing the crack opening parameters before and after the healing. The irregular shape of the crack tends to reduce the accuracy of pointwise measures (e.g. manual width measurements). On the other hand, the main advantage of image processing consists in allowing to obtain a continuous estimation of a given chosen parameter all along the crack. Measuring the self-sealing under several different conditions requires

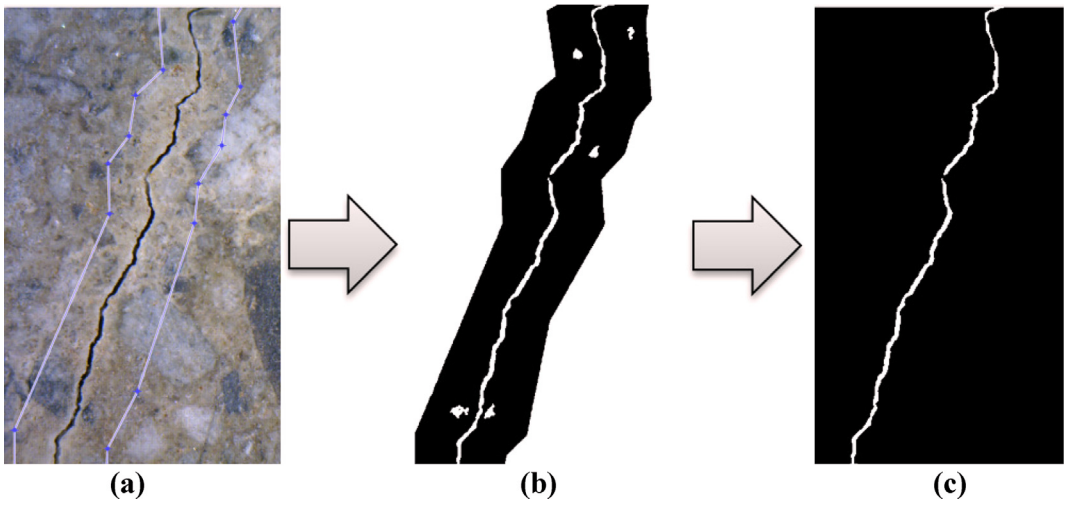

Fig. 8. Image processing for crack area detection: (a) crack region definition, (b) image binarization output, (c) final output.

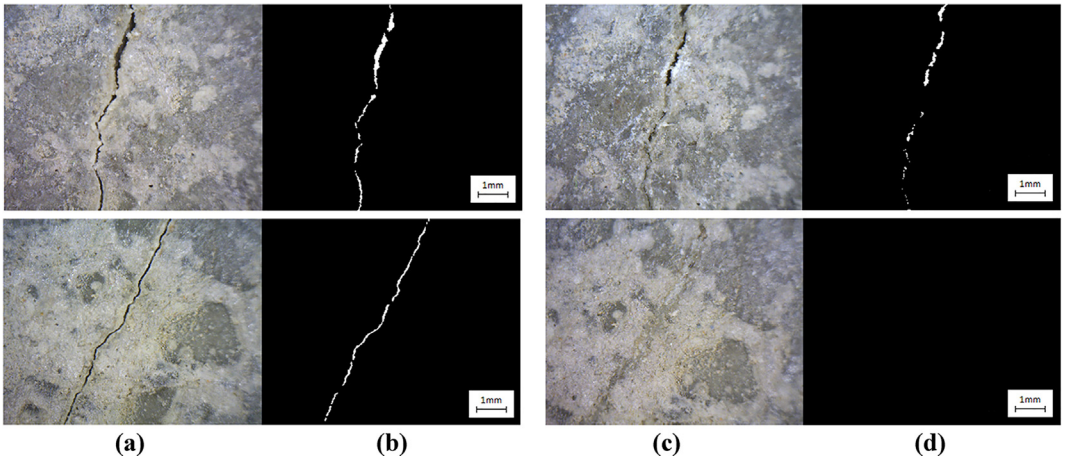

Fig. 9. (a) Original image after cracking. (b) Binary image after cracking. (c) Original image after healing treatment. (d) Binary image after healing treatment.

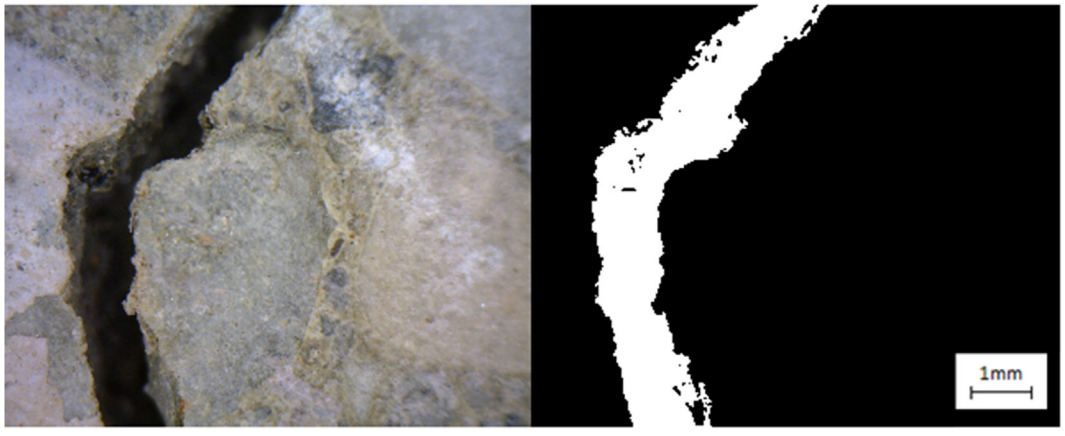

Fig. 10. Light reflection on the crack inner walls.

identifying the crack width or surface and comparing it along the different stages of the cracking-healing process.

The algorithm described hereafter gives a procedure to detect the crack and to garner information about its surface in image units (pixels). A fully-automated solution requires a uniform texture for the whole image dataset. In this case, the variety of concrete surfaces (Fig. 6) requires a semiautomatic thresholding as well as a semiautomatic outlier removal. The procedure shown in Fig. 7 was implemented in MATLAB, taking advantage of the Image Processing Toolbox default functions.

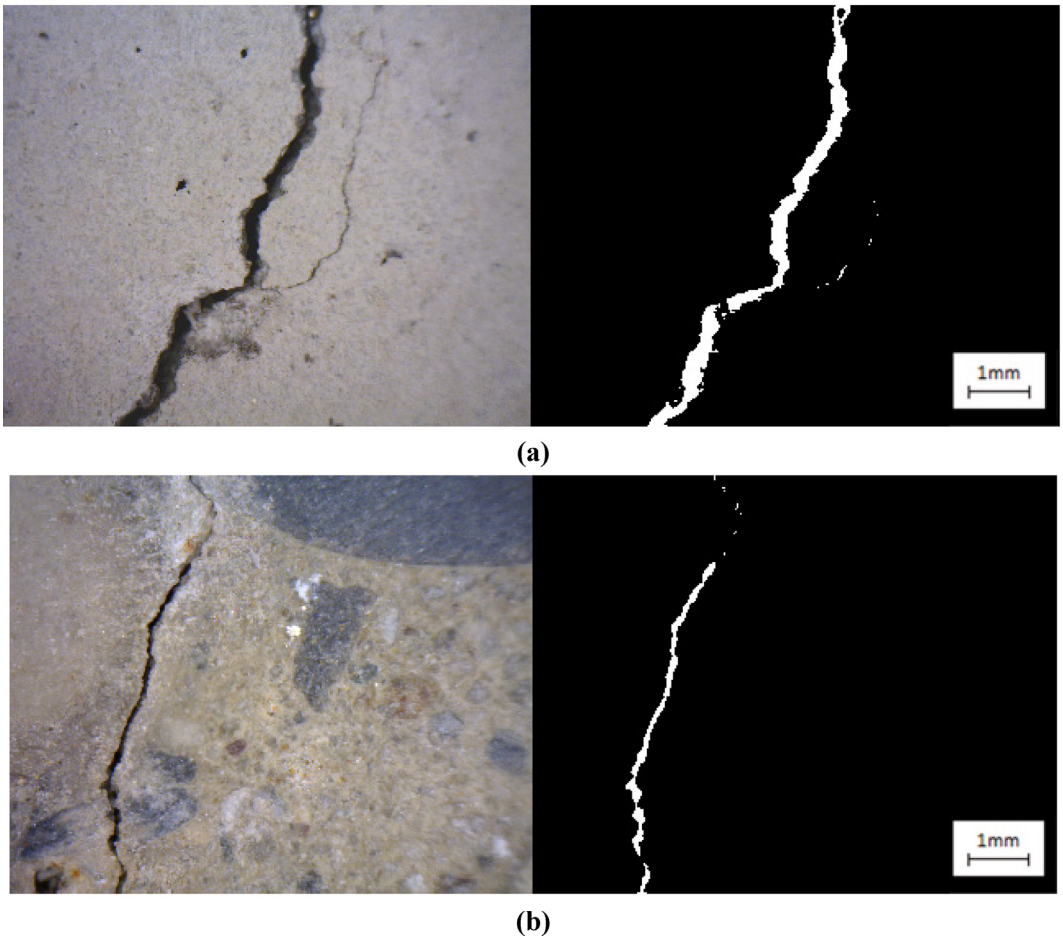

Fig. 11. Images corresponding to the widest crack of the crack width ranges under consideration: (a) medium cracks (0.30–0.15 mm) and (b) small cracks (<0.15 mm).

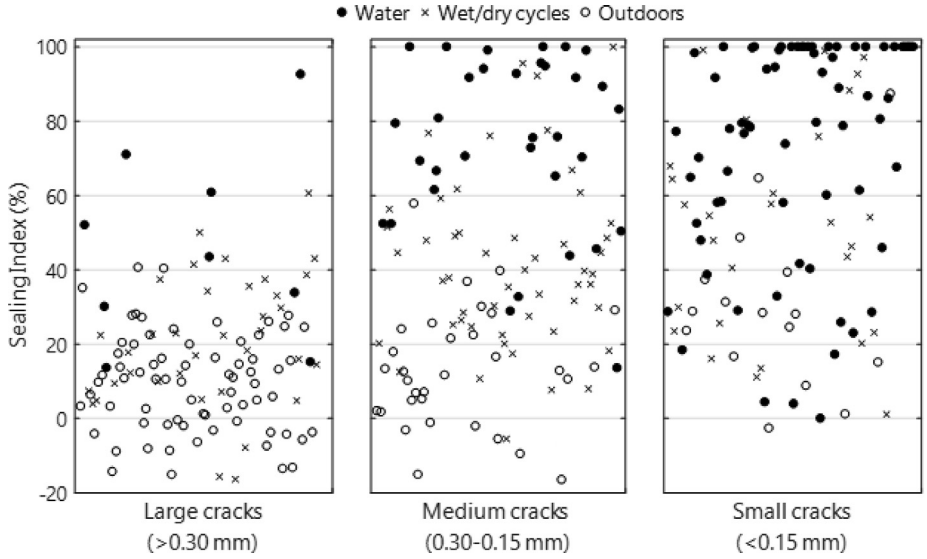

Fig. 12. Sealing index for the various crack widths as a function of the exposure conditions. Each observation corresponds to a specimen after a particular healing treatment.

The image intake was carried out using a digital microscope Dino-Lite Pro AM413ZT. Four images at each side of the crack were taken, making a total of eight images for each specimen both after the pre-cracking and after each corresponding healing treatment.

In order to extract the crack area from each image, a semiautomatic procedure was implemented in MATLAB. The image processing method is based on three major steps: image pre-processing, image binarization and outlier removal. Fig. 8 illustrates the proposed methodology. The pre-processing starts by transforming the image from RGB (TrueColor image: Red, Green, Blue) to greyscale and selecting the area which contains the target crack (Fig. 8a). It is thus possible to avoid significant artifacts such as spurious incorporation of secondary cracks into the analysis. Subsequently, a low-pass filter is applied in order to reduce the image noise. The image binarization (Fig. 8b) then follows through which each pixel is assigned one of two possible values, "1" for pixels belonging to the crack or "0" for those pix-els outside the crack. In particular, the method here applied is known as "adaptive thresholding" [57]. This algorithm computes a locally adaptive threshold for each pixel using the local mean intensity around the neighborhood of the pixel. Morphological operations such as dilation and erosion allow for outlier removal. The pixels misclassified as crack are filtered by means of region erosion, whereas the pixels misclassified as non-crack are corrected using the dilation operation (Fig. 8c). Fig. 9 shows a comparison between cracks, image analyzed as above, after the pre-cracking test (Fig. 9a-b) and after the subsequent healing period (Fig. 9c-d).

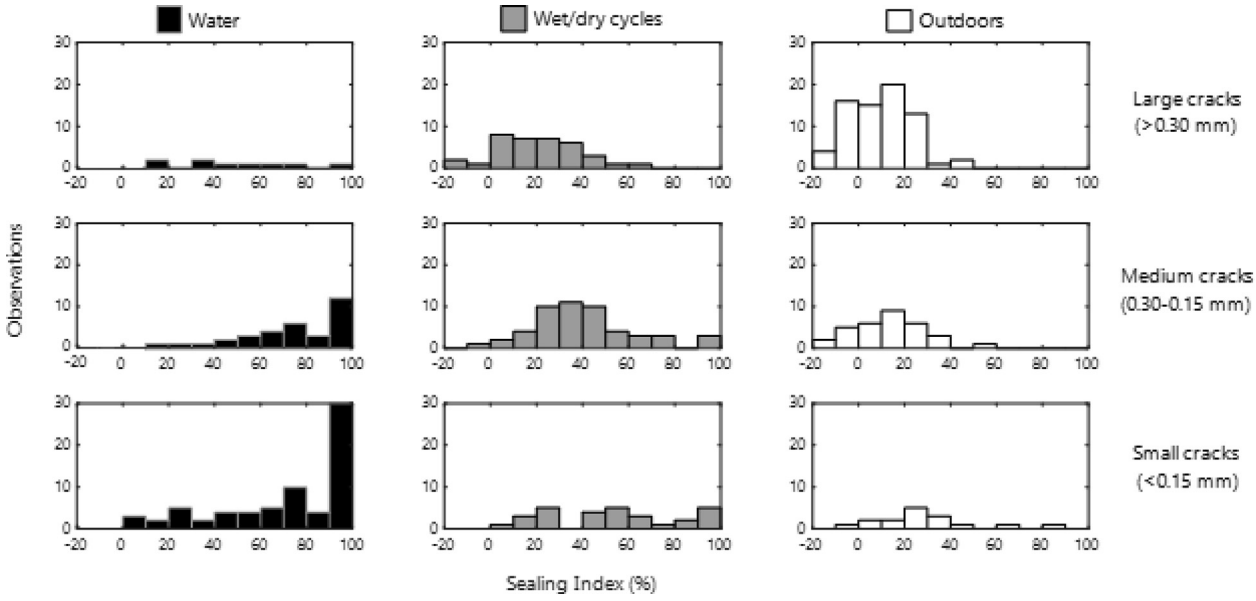

Fig. 13. Histograms showing the number of observations (vertical axis) reaching a certain Sealing Index % (horizontal axis) as a function of the crack width and the environmental exposure.

Table 4
Basic statistics of the Sealing Index for the samples containing (a) fibers parallel to the critical section and (b) fibers perpendicular to the critical section (fracture plane) as a function of the mix design and the environmental exposure.

Sealing Index (%)	Fibers parallel to the critical section (H2,V1,V2,V3)					
	Reference Concrete (without crystalline admixtures)			C.A. Concrete (with crystalline admixtures)		
	Water	Wet/dry cycles	Open-air	Water	Wet/dry cycles	Open-air
Min	0	1.07	−15.12	4.38	−5.48	−16.48
Max	100	100	57.84	100	60.68	35.12
Mean	**73.64**	**46.31**	**8.774**	**77.83**	**28.52**	**9.76**
Median	80.50	44.51	6.98	81.96	27.49	10.99
St. Deviation	30.33	29.41	17.23	23.83	14.57	14.07
(a)						
Sealing Index (%)	Fibers perpendicular to the critical section (H1,H3)					
	Reference Concrete (without crystalline admixtures)			C.A. Concrete (with crystalline admixtures)		
	Water	Wet/dry cycles	Open-air	Water	Wet/dry cycles	Open-air
Min	18.40	7.67	−9.56	7.01	−16.31	−5.54
Max	100	99.17	87.37	100	95.62	31.34
Mean	**70.31**	**47.37**	**20.43**	**54.70**	**27.56**	**13.27**
Median	77.90	46.59	16.63	52.03	29.04	12.70
St. Deviation	24.75	26.66	22.25	35.41	30.34	10.74
(b)						

A database containing information of more than 6300 images was developed. The subsequent data analysis allowed for determining the crack sealing capacity in correspondence to each relevant variable (including e.g. the environmental exposure and the mix composition).

As already described, the specimens were photographed using a digital microscope both at the beginning and at the end of each healing treatment. The crack sealing capacity was quantified by means of the crack surface closure after each healing treatment. The percentage of crack closure after each healing period is also referred to as the Sealing Index (S.I.), and is calculated as follows, for specimen i after the healing treatment j, Eq. (1):

$$Sealing\ Index^{j}{}_{i} = \frac{\sum_{1}^{8} CA^{j-1}_{i,cracked} - \sum_{1}^{8} CA^{j}_{i,healed}}{\sum_{1}^{8} CA^{j-1}_{i,cracked}} \cdot 100 \quad (1)$$

where $\sum_{1}^{8} CA^{j-1}{}_{i,cracked}$, is the lump sum of the crack area in the 8 images of the sample i, taken right after the cracking performed at the end of the healing treatment j-1.

$\sum_{1}^{8} CA^{j-1}{}_{i,healed}$, is the lump sum of the crack area in the images of the sample i, at the end of the healing treatment j.

The observation of the cracks all along the experimental campaign aimed to evaluate the influence of several variables in the self-sealing phenomena. In the DEWS test the sample was loaded up to an average COD equal to 0.25 mm at each step, similar as in [56]. However, larger cracks may occur due to sporadic out-of-plane rotations during the test. As already shown in [2,58], a complete sealing is hard to be reach for cracks wider than 0.20 mm. In addition, the utilized image processing method becomes less effective for cracks larger than 0.50 mm. In these cases, the inclination of the internal edges of the crack (bevel effect) is more prominent compared to smaller cracks and it could complicate the automation process due to the fact that the light is also reflecting inside the crack inner walls, thus disturbing the appropriate image binarization (Fig. 10). Another reason for including the initial crack width as an influence parameter on the crack closure is related to the mix design. In particular, it was important to determine whether the crystalline admixture improves the self-sealing capacity with respect to the reference concrete (without crystalline admixtures) for small and/or for large cracks.

In order to evaluate the self-sealing performance as a function of the crack width, the following arrangement of the image-processed data was proposed. The whole set of data was discretized in three different categories: large cracks, medium cracks and small cracks. By measuring the average width of the largest crack in each of the bins, it is possible to match these categories to a certain crack width range. The first group ranges from a crack width of about 2.5 mm, which corresponds to the largest measured value, to roughly 0.3 mm (maximum crack width generally allowed by design codes). The second group contains cracks from

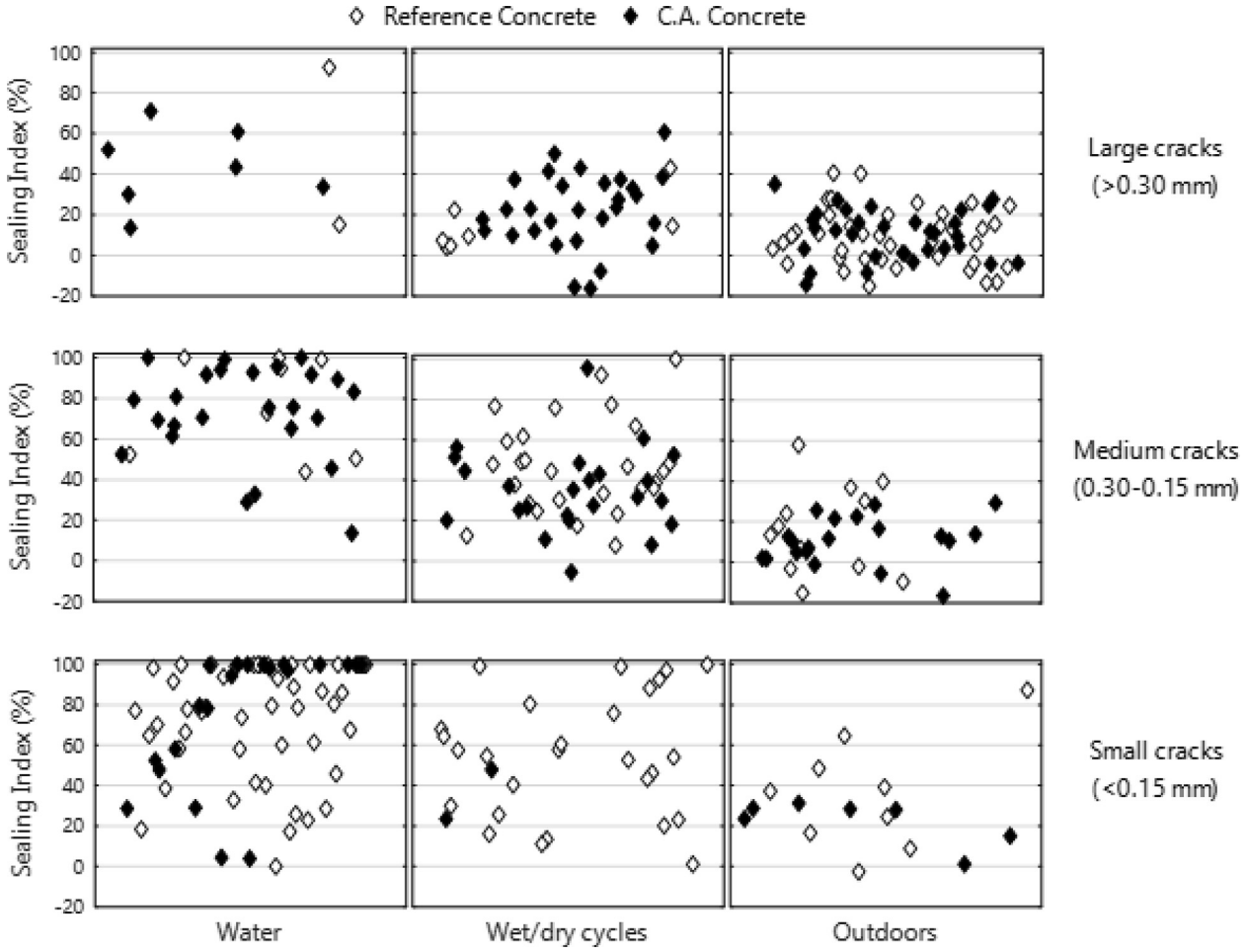

Fig. 14. Sealing index as a function of the crack width, the environmental exposure and the mix design.

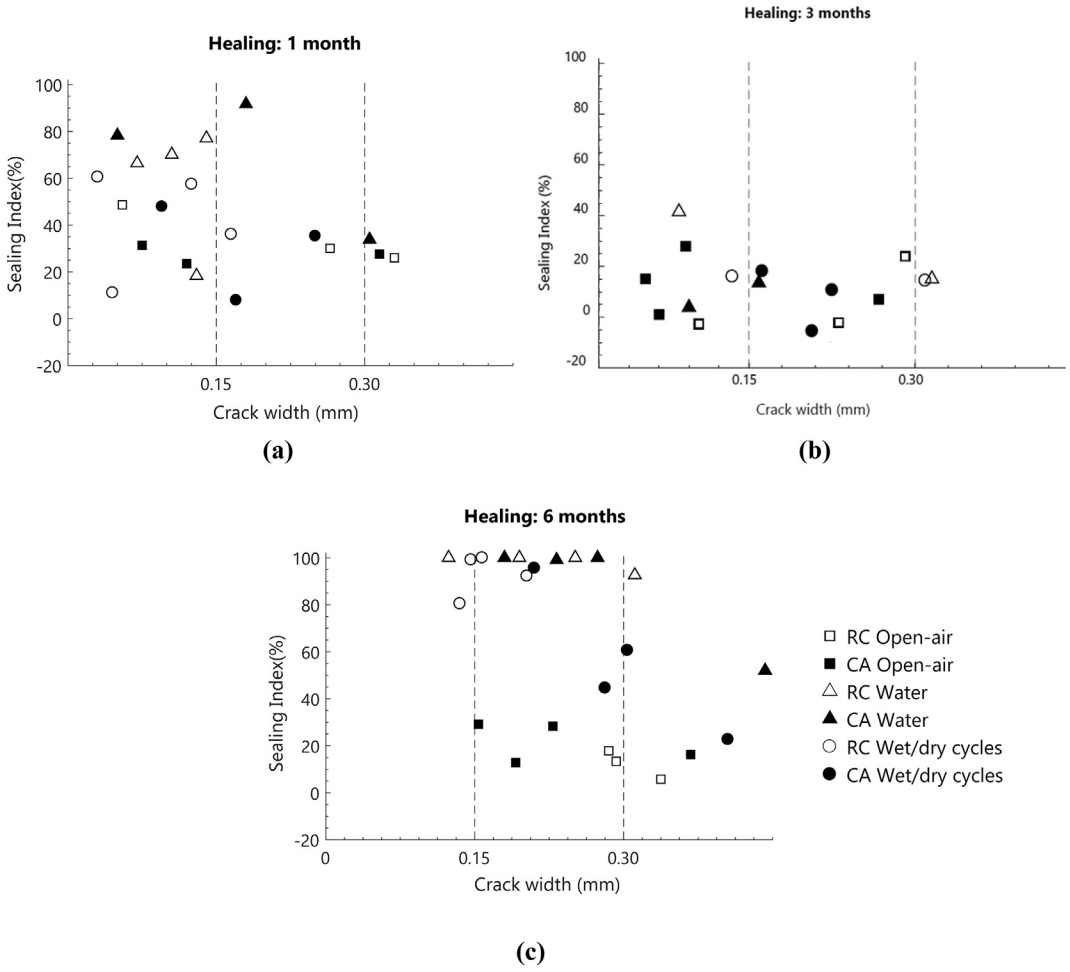

Fig. 15. Sealing Index (%) for the first healing treatment of (a) 1 month, (b) 3 months and (c) 6 months, as a function of the crack width, the exposure conditions and the mix design (RC: Reference concrete; CA: Concrete with crystalline admixtures).

about 0.3 mm wide, as the one shown in Fig. 11a, to 0.15 mm, which is also the top width of the group containing the smallest cracks, represented in Fig. 11b. Crack widths between 0.15 and 0.3 mm are generally allowed under serviceability conditions, while for highly aggressive environments, crack widths should not exceed 0.15 mm.

3. Results

3.1. Crack sealing evaluation

The sealing index calculated as in Eq. (1) has been plotted in Fig. 12 for the three defined ranges of crack opening. First, it can be observed that the complete sealing for large cracks (>0.30 mm) was not reached even for permanent water immersion.

Open-air exposed specimens featured larger cracks, because of the lower effectiveness of sealing capacity. On the other hand, for permanent water-immersion instead, most of the observations featured cracks narrower than 0.15 mm. Regardless, whether the samples did or did not heal during a certain healing treatment, a new DEWS cracking test was performed, repeatedly enlarging the crack (the crack was opened an additional 0.25 mm) at each cycle. Hence, those samples with a scarce sealing continued increasing their crack opening after each splitting test, whereas those undergoing a successful crack sealing always remained in the lower crack opening ranges. As shown in Fig. 13, for cracks narrower than 0.15 mm and specimens being permanently immersed in water, the most frequent result was the complete sealing of the crack. Open-air exposure samples showed a low performance regardless of the crack width, whilst wet/dry samples featured an average recovery of 41% for medium cracks and 53% for small cracks.

Regarding the fiber orientation, it seemed to have no influence on the self-sealing, as indicated in Table 4. The influence of the crystalline admixture is difficult to be ascertained when observing the complete range of crack widths. When splitting the observations according to the crack width and environmental exposure, it clearly appears that the crystalline admixture result in a significant improvement of the crack sealing performance for small cracks when permanently immersed in water (Fig. 14). Under these conditions, only 38% of the Reference Concrete (without crystalline admixture) observations showed complete sealing, whereas the specimens made with C.A. Concrete (with crystalline admixture) healed the crack completely in 55% of the cases.

In Table 4, each Standard Deviation value corresponds to three constant parameters: similar fiber orientation, environmental exposure (water, cycles or open air exposure) and type of concrete (with or without crystalline admixture). However, within each value there are the following variables: different position of the DEWS specimen within its prismatic specimen, different crack opening values and different durations of the healing period. If these variables are combined with the inherent variability of the

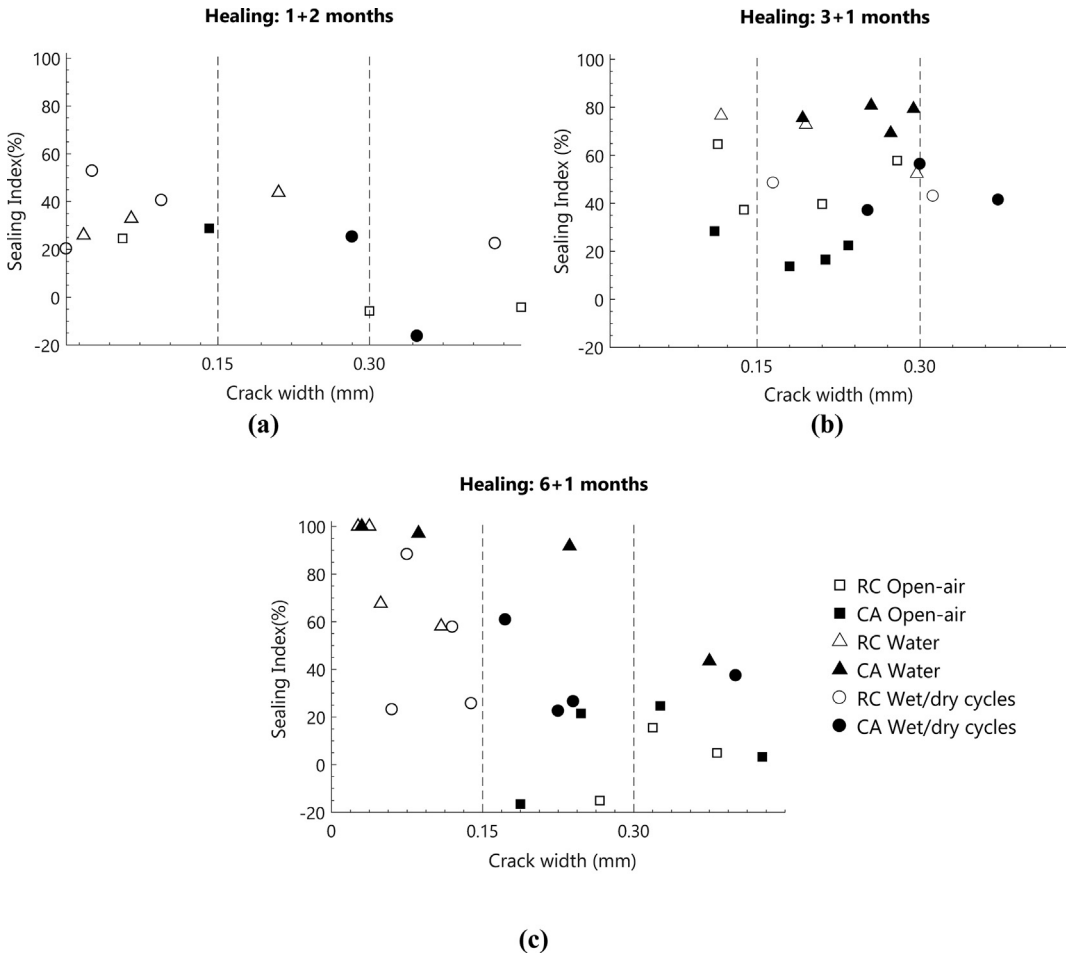

Fig. 16. Sealing Index for the second healing treatment of (a) 2 months, (b) 1 month and (c) 1 month, as a function of the crack width, the exposure conditions and the mix design (RC: reference concrete; CA: concrete with crystalline admixtures).

tensile tests, the values of variability (Standard Deviation) are acceptable.

In order to better understand the self-sealing capacity provided by the crystalline admixtures it is necessary to study its performance along the entire experimental campaign. The proposed experimental schedule allows for analyzing the first healing treatment response for different durations. As explained in Fig. 15 three experimental paths were considered with reference to the duration of the first treatment, respectively a 1 month-long treatment (FT-1), a 3 month-long treatment (FT-3) and a 6 month-long treatment (FT-6). The results of the first and second healing treatments are shown in Figs. 15 and 16 respectively. The specimens undergoing a 6 month-long healing (Fig. 15c) outperform the rest of the observations. Moreover, by observing the subsequent healing treatment for each of the experimental paths (Figs. 15 and 17), the FT-6 samples (Fig. 15c) exhibited a better performance when compared to FT-1 (Fig. 15a) and FT-3 (Fig. 15b) specimens. Therefore, a longer initial healing period may induce a better self-sealing performance for later cracking. This may be due to osmotic movement of the crystalline molecules towards the crack where they are consumed by the healing reactions. The effect of a longer initial treatment is also shown in Fig. 17, showing the entire yearlong experimental results for water-immersed specimens having cracks narrower than 0.15 mm.

The three experimental paths are represented in Fig. 17, where both the average Sealing Index and its standard deviation are given at each age of observation. By analyzing the entire experimental campaign over time, it is possible to state that the self-sealing capacity of the Reference Concrete (without crystalline admixtures) decreased at the age of one year. The observed trend seems to indicate that, after an entire year of cracking-healing cycles, the unhydrated cement particles, which are naturally contained in the concrete, allowing the autogenous self-sealing, start to be consumed, regardless of the initial healing period. On the other hand, the concrete containing crystalline admixtures continued to guarantee higher performances even after several cracking-healing cycles. Additionally, the effect of a different cracking-healing background (FT-1, FT-3 and FT-6 differ only in the first semester of the experimental campaign) tends to vanish if followed by a regular cracking-healing scheme (Fig. 5).

3.2. SEM and EDS analyses

SEM observations were carried out, on samples collected from crack surfaces of two additional concrete specimens, respectively with and without crystalline admixture, after 3 months of immersion in water (Figs. 18 and 19).

It can be observed that the morphology of hydration products is similar to that typical of an ordinary concrete (without crystalline admixtures, Fig. 19) and to the one with crystalline admixtures shown in Fig. 18. Also EDS analysis carried out on the zone highlighted in Figs. 18 and 19 confirms the absence of the sulphur peak. For the sample with crystalline admixtures the cement matrix was

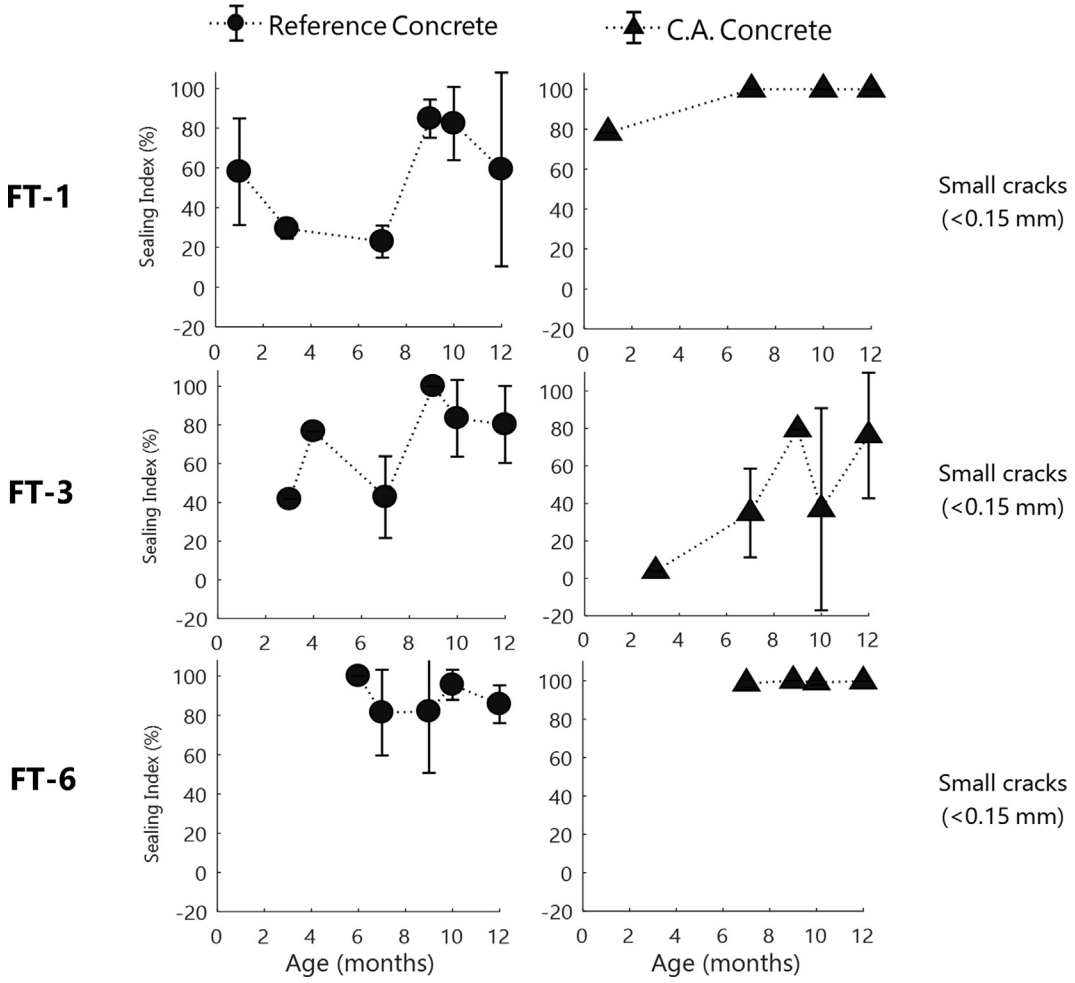

Fig. 17. Comparison of the Sealing Index progression over time for small cracks when immersed permanently in water as a function of the mix design and the experimental schedule (sample groups FT-1, FT-3 and FT-6).

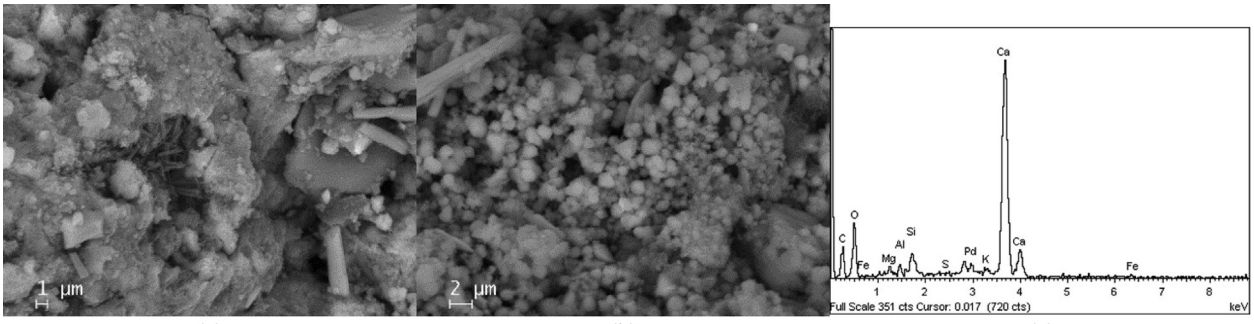

Fig. 18. SEM images (a), (b) and EDS analysis (c) of a sample of concrete with crystalline admixture immersed in water for 3 months.

covered with very fine acicular products (Fig. 18a-b). The morphology of these products is compatible with the crystalline structure of typical self-healing products; several authors [19,59,60] have observed similar acicular products which were identified as very common microstructures found in self-healed samples, specifically some ettringite crystals (hydrous calcium aluminium sulfate mineral) were formed inside and filled the cracks.

EDS analysis of the products in Fig. 18c shows mainly the typical elements of hydration products of cement (calcium, oxygen and silicon in major amounts, in addition to magnesium, aluminum and potassium).

Fig. 19 shows the case of concrete without crystalline admixtures in which the healing product has exclusively a cubic shape and no filaments are observed. Based on EDS, the precipitation (healing product) mainly consisted of $CaCO_3$. This precipitation adopted cubic forms in the case of concrete without crystalline admixture (Fig. 18) and, in the case of concrete with crystalline admixture (Fig. 19) adopted cubic and acicular forms.

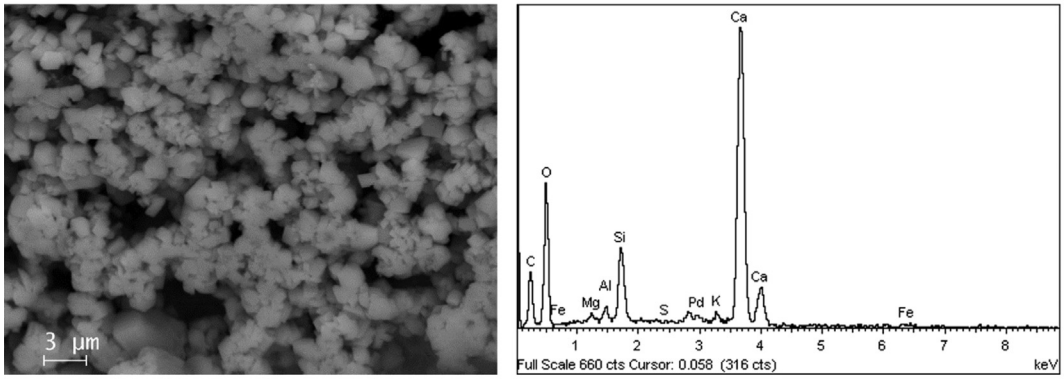

Fig. 19. SEM image (a) and EDS analysis (b) of a sample of concrete without crystalline admixture immersed in water for 3 months.

4. Conclusions

The main goal of this paper was to propose and validate a methodology to evaluate the self-sealing capacity of a steel-fiber reinforced concrete over several repeated cracking and healing cycles and to study the influence of a crystalline admixture employed as a healing stimulator. The specimens were cracked by means of Double Edge Wedge Splitting (DEWS) tests and cured under three different conditions: water immersion, open-air exposure and wet/dry cycles to be healed. Crack images were garnered for each specimen all along the investigated path and crack width parameters were evaluated through image processing by means of a semiautomatic method, developed using MATLAB Image Analysis Toolbox function. This method has given very valuable information about the self-sealing on the surface of the crack.

Based on the described research, the following conclusions can be stated:

- The environmental exposure is the most determinant factor for the self-sealing capacity. Open-air exposure specimens exhibit a low crack sealing. On the other hand, the most frequent result for water-immersed specimens is the complete sealing of the cracks even under repeated cracking and healing cycles and up to one year after the first cracking.
- The complete sealing of the crack is only observed for specimens permanently or periodically immersed in water and having crack widths below 0.30 mm.
- The self-sealing enhancement induced by the crystalline admixtures is most relevant in narrow cracks up to 0.15 mm wide, when permanently immersed in water. The effect of the crystalline admixture persists after repeated cracking-healing cycles up to one year.
- On the contrary the self-sealing capacity of the Reference Concrete after repeated cracking-healing cycles, starts decreasing after 1 year, regardless of the experimental background. This might be due to the consumption of the products that are naturally contained in the concrete allowing for the autogenous self-sealing.
- The influence of the fiber orientation on the self-sealing capacity is almost nil. Even when fibers are preferentially oriented perpendicular to the crack, no enhancement of the crack sealing is observed. This can be due to the low dosage of steel fibers (0.51% by volume)
- A longer initial treatment may induce a better self-sealing capacity against later cracking, especially when a crystalline admixture is added to the mix to stimulate the healing. This may be due to osmotic movement of the crystalline molecules towards the crack where they are consumed by the healing reactions.
- SEM observations and EDS analyses confirmed the presence of healing products on the healed surfaces. These products were due to the delayed hydration and carbonation reactions involving both the cement and the crystalline admixture. The morphology of these products and their relative EDS analysis also suggest that some ettringite crystals (hydrous calcium aluminium sulfate mineral) may form inside and fill the same cracks.

Conflict of interest

The authors declare that they have no conflict of interest.

Acknowledgements

The authors acknowledge the financial support of the PoliMi International Fellowships 2015 (PIF) and acknowledge the cooperation and financial support of Penetron Italia, Ltd., MArch. Enricomaria Gastaldo Brac.

References

[1] M. De Rooij, K. Van Tittelboom, N. De Belie and E. Schlangen, Self-Healing Phenomena in Cement-Based Materials. State-of-the-Art Report of RILEM Technical Committee 221-SHC: Self-Healing Phenomena in Cement-Based Materials, Springer, 2013.
[2] C. Edvarsen, Water permeability and autogenous healing of cracks in concrete, ACI Mater. J. 96 (4) (1999) 448–454.
[3] D. Homma, H. Mihashi, T. Nishiwaki, Self-healing capability of fibre reinforced cementitious composites, J. Adv. Concr. Tecnol. 7 (2) (2009) 217–228.
[4] K. Van Tittelboom, E. Gruyaert, H. Rahier, N. De Belie, Influence of mix composition on the extent of autogenous crack healing by continued hydration or calcium carbonate formation, Constr. Build. Mater. 37 (2012) 349–359.
[5] Y. Yang, M. Lepech, E. Yang, V. Li, Autogenous healing of engineered cementitious composties under wet-dry cycles, Cem. Concr. Res. 39 (2009) 382–390.
[6] L. Ferrara, V. Krelani, F. Moretti, M. Roig-Flores, P. Serna, Effects of autogenous healing on the recovery of mechanical performance of High Performance Fibre Reinforced Cementitious Composites (HPFRCCs): part 1, Cem. Concr. Compos. 83 (2017) 76–100.
[7] L. Ferrara, V. Krelani, F. Moretti, Autogenous healing on the recovery of mechanical performance of High Performance Fibre Reinforced Cementitious Composites (HPFRCCs): part 2 - correlation between healing of mechanical performance and crack sealing, Cem. Concr. Compos. 73 (2016) 299–315.
[8] D. Snoeck, Self-healing and microstructure of cementitious materials with microfibres and superabsorbent polymers, Ghent University: Doctor in Civil Engineering: Construction Design, 2015.
[9] D. Snoeck, N. De Belie, From straw in bricks to modern use of microfibers in cementitious composites for improved autogenous healing–a review, Constr. Build. Mater. 95 (2015) 774–787.

[10] E. Cuenca, L. Ferrara, Self-healing capacity of fiber reinforced cementitious composites. State of the art and perspectives, KSCE J. Civ. Eng. 21 (7) (2017) 2777–2789.
[11] L. Ferrara, V. Krelani, F. Moretti, On the use of crystalline admixtures as promoters of self-healing in cement based construction materials, Smart Mater. Struct. 25 (8) (2016).
[12] M. Roig-Flores, S. Moscato, P. Serna, L. Ferrara, Self-healing capability of concrete with crystalline admixtures in different environments, Constr. Build. Mater. 86 (2015) 1–11.
[13] K. Van Tittelboom, D. Snoeck, J. Wang and N. De Belie, Most recent advances in the field of self-healing cementitious materials, in: ICSHM 2013: Proceedings of the 4th International Conference on Self-Healing Materials, Ghent, Belgium, 2013.
[14] M. Wu, B. Johannesson, M. Geiker, A review: Self-healing in cementitious materials and engineered cementitious composite as a self-healing material, Constr. Build. Mater. 28 (2012) 571–583.
[15] K. Van Tittelboom, N. De Belie, Self-healing in cementitious materials – a review, Materials 6 (6) (2013) 2182–2217.
[16] L. Ferrara, T. Van Mullem, M. Alonso, P. Antonaci, R. Borg, E. Cuenca, A. Jefferson, P. Ng, A. Peled, M. Roig, M. Sanchez, C. Schroefl, P. Serna, D. Snoeck, J. Tulliani, N. De Belie, Experimental characterization of the self-healing capacity of cement based materials and its effects on the material performance: a state of the art report by COST Action SARCOS WG2, Constr. Build. Mater. 167 (2018) 115–142.
[17] T. Nishiwaki, H. Sasaki, S. Kwon, G. Igarashi, H. Mihashi, Experimental study on self-healing effect of FRCC with PVA fibers and additives against freeze/thaw cycles, in: ICSHM, 2015.
[18] L. Ferrara, S. Ferreira, V. Krelani, M. Della Torre, F. Silva, R. Toledo, Natural fibers as promoters of autogenous healing in HPFRCCs: Results from on-going Brazil-Italy cooperation, ACI Special Publication 305 (11) (2015) 1–10.
[19] L. Ferrara, V. Krelani, M. Carsana, A fracture testing based approach to assess crack healing of concrete with and without crystalline admixtures, Constr. Build. Mater. 68 (2014) 535–551.
[20] M. Roig-Flores, F. Pirritano, P. Serna, L. Ferrara, Effect of crystalline admixtures on the self-healing capability of early-age concrete studied by means of permeability and crack closing tests, Constr. Build. Mater. 114 (1) (2016) 447–457.
[21] R. Borg, E. Cuenca, E. GastaldoBrac, L. Ferrara, Crack sealing capacity in chloride-rich environments of mortars containing different cement substitutes and crystalline admixtures, J. Sustainable Cem.-Based Mater. (2017) 1–19.
[22] D. Snoeck, N. De Belie, Repeated autogenous healing in strain-hardening cementitious composites by using superabsorbent polymers, J. Mater. Civ. Eng. 28 (1) (2015) 1–11.
[23] D. Snoeck, J. Dewanckele, V. Cnudde, N. De Belie, X-ray computed microtomography to study autogenous healing of cementitious materials promoted by superabsorbent polymers, Cem. Concr. Compos. 65 (2016) 83–93.
[24] D. Snoeck, K. Van Tittelboom, S. Steuperaert, P. Dubruel, N. De Belie, Self-healing cementitious materials by the combination of microfibers and superabsorbent polymers, J. Intell. Mater. Syst. Struct. 25 (1) (2014) 13–24.
[25] E. Cuenca, J. Echegaray-Oviedo, P. Serna, Influence of concrete matrix and type of fiber on the shear behavior of self-compacting fiber reinforced concrete beams, Compos. B Eng. 75 (2015) 135–147.
[26] F. Ortiz-Navas, J. Navarro-Gregori, G. Leiva-Herdocia, P. Serna, E. Cuenca, An experimental study on the shear behaviour of reinforced concrete beams with macro-synthetic fibres, Constr. Build. Mater. 169 (2018) 888–899.
[27] E. Cuenca, A. Conforti, F. Minelli, G. Plizzari, J. Navarro-Gregori, P. Serna, A material-performance-based database for FRC and RC elements under shear loading, Mater. Struct. 51 (1) (2018).
[28] M. DiPrisco, G. Plizzari, L. Vandewalle, MC2010: overview on the shear provisions for FRC. Fib bulletin 57, Fib Bulletin 57 57 (2010) 61–76.
[29] J. Susetyo, F. Vecchio, Effectiveness of the steel fiber as minimum shear reinforcement: panel test, Fib bulletin 57 57 (2010) 227–241.
[30] E. Cuenca, P. Serna, Shear behavior of prestressed precast beams made of self-compacting fiber reinforced concrete, Constr. Build. Mater. 45 (2013) 145–156.
[31] A. Conforti, G. Tiberti, G. Plizzari, Splitting and crushing failure in FRC elements subjected to a high concentrated load, Compos. B Eng. 105 (2016) 82–92.
[32] K. Kim, D. Lee, J. Hwang, D. Kuchma, Shear behavior model for steel fiber-reinforced concrete members without transverse reinforcements, Compos. B Eng. 43 (5) (2012) 2324–2334.
[33] E. Cuenca, P. Serna, Failure modes and shear design of prestressed hollow core slabs made of fiber-reinforced concrete, Compos. B Eng. 45 (1) (2013) 952–964.
[34] M. Mousa, E. Cuenca, L. Ferrara, N. Roy, A. Tagnit-Hamou, Tensile characterization of an "Eco-friendly" UHPFRC with waste glass powder and glass sand, in: SHCC 2017: Strain-Hardening Cement-Based Composites, RILEM Bookseries, 2018, pp. 238–248.
[35] F. Bencardino, L. Rizzuti, G. Spadea, R. Swamy, Experimental evalutation of fiber reinforced concrete fracture properties, Compos. B Eng. 41 (1) (2010) 17–24.
[36] A. Conforti, F. Minelli, Compression field modelling of fibre reinforced concrete shear critical deep beams: a numerical study, Mater. Struct. 49 (8) (2016) 3369–3383.
[37] J. Echegaray-Oviedo, J. Navarro-Gregori, E. Cuenca, P. Serna, Modified push-off test for analysing the shear behaviour of concrete cracks, Strain 53 (6) (2017).
[38] V. Li, S. Wang, C. Wu, Tensile strain-hardening behavior of polyvinyl alcohol engineered cementitious composites (PVA-ECC), ACI Mater. J. 98 (1997) 483–492.
[39] M. Sahmaran, G. Yildirim, R. Noori, E. Ozbay, M. Lachemi, Repeatability and pervasiveness of self-healing in engineered cementitious composites, ACI Mater. J. 112 (4) (2015) 513–522.
[40] M. Li, S. Fan, Designing repeatable Self-healing into cementitious materials, in: 5th International Conference on Durability of Concrete Structures, China, 2016.
[41] E. Cuenca, L. Ferrara, Effects of crystalline admixtures on the repeatability of self healing in fiber reinforced concrete, Constr. Mater. Syst. 5 (163) (2017).
[42] E. Cuenca, L. Ferrara, Repeatability of self-healing in fiber reinforced concretes with and without crystalline admixtures: preliminary results, ACI Special Publication 319 (11) (2017) 1–18.
[43] A. Mohan, S. Poobal, Crack detection using image processing: A critical review and analysis, Alexandria Eng. J. (2017).
[44] T. Hutchinson, Z. Chen, Image-based framework for concrete surface crack monitoring and quantification, Adv. Civ. Eng. (2010).
[45] S. Kulkarni, Filtering and enhancement, in: ELE201 Introd. to Electr. Signals Syst., 2002, pp. 1–12.
[46] O. ImochaSingh, T. Sinam, O. James, T. RomenSingh, Local contrast and mean thresholding in image binarization, Int. J. Comput. Appl. 51 (6) (2012) 4–10.
[47] T. RomenSingh, S. Roy, K. ManglemSingh, Local adaptive automatic binarisation (LAAB), Int. J. Comput. Appl. 40 (6) (2012) 27–30.
[48] A. Talab, Z. Huang, F. Xi, L. Haiming, Detection crack in image using Otsu method and multiple filtering in image processing techniques, Optik 127 (3) (2016) 1030–1033.
[49] E. Dougherty, R. Lotufo, Hands-on morphological image processing, 59, 2003.
[50] R. Adhikari, O. Moselhi, A. Bagchi, Image-based retrieval of concrete crack properties for bridge inspection, Autom. Constr. 39 (2014) 180–194.
[51] B. Lee, Y. Kim, S. Yi, J. Kim, Automated image processing technique for detecting and analysing concrete surface cracks, Struct. Infrastruct. Eng. 9 (6) (2013) 567–577.
[52] W. Zhang, Z. Zhang, D. Qi, Y. Liu, Automatic crack detection and classification method for subway tunnel safety monitoring, Sensors 14 (10) (2014) 19307–19328.
[53] M. Jahanshahi, S. Masri, C. Padgett, G. Sukhatme, An innovative methodology for detection and quantification of cracks through incorporation of depth perception, Mach. Vis. Appl. 24 (2) (2013) 227–241.
[54] Y. Fujita, Y. Hamamoto, A robust automatic crack detection method from noisy concrete surfaces, Mach. Vis. Appl. 22 (2) (2011) 245–254.
[55] J. Valença, D. Dias-Da-Costa, E. Júlio, H. Araújo, H. Costa, Automatic crack monitoring using photogrammetry and image processing, Measurement 46 (1) (2013) 433–441.
[56] M. DiPrisco, L. Ferrara, M. Lamperti, Double edge wedge splitting (DEWS): an indirect tension test to identify post-cracking behaviour of fibre reinforced cementitious composites, Mater. Struct. 46 (2013) 1893–1918.
[57] D. Bradley, G. Roth, Adaptive thresholding using the Integral Image, J. Graph. Tools 12 (2) (2007) 13–21.
[58] Y. Yang, E. Yang, V. Li, Autogenous healing of engineered cementitious composites at early age, Cem. Concr. Res. 41 (2) (2011) 176–183.
[59] R. Gagné, M. Argouges, A study of the natural self-healing of mortars using air-flow measurements, Mater. Struct. 45 (2012) 1625–1638.
[60] K. Sisomphon, O. Copuroglu, Self healing mortars by using different cementitious materials, in: Proc. Intl. Conf. on Advances in Construction Materials Through Science and Engineering, Hong Kong, China, 2011.